

High Magnetoresistance Ratio on hBN Boron-Vacancy/Graphene Magnetic Tunnel Junction

Halimah Harfah,^{1,*} Yusuf Wicaksono,^{2,†} Gagus Ketut Sunnardianto,^{3,4} Muhammad Aziz Majidi,⁵ and Koichi Kusakabe⁶

¹*Graduate School of Engineering Science, Osaka University, 1-3 Machikaneyama-Cho, Toyonaka, Osaka 560-0043, Japan*

²*Computational Condensed Matter Physics Laboratory, RIKEN, 2-1 Hirosawa, Wako, Saitama 351-0198, Japan*

³*Research Center for Quantum Physics, National Research and Innovation Agency (BRIN), Tangerang Selatan, Banten, 15314, Indonesia*

⁴*Research Collaboration Center for Quantum Technology 2.0, Bandung 40132, Indonesia*

⁵*Department of Physics, Faculty of Mathematics and Natural Science, Universitas Indonesia, Kampus UI Depok, Depok 16424, Indonesia.*

⁶*School of Science, Graduate School of Science, University of Hyogo 3-2-1 Kouto, Kamigori-cho, Ako-gun, 678-1297, Hyogo, Japan.*

(Dated: December 25, 2023)

We presents a new strategy to create a van der Waals-based magnetic tunnel junction (MTJ) that consists of a three-atom layer thickness of graphene (Gr) sandwiched with hexagonal boron nitride (hBN) by introducing a monoatomic Boron vacancy in both hBN layers. The magnetic properties and electronic structure of the system were investigated using density functional theory (DFT), while the transmission probability of the MTJ was investigated using the Landauer-Büttiker formalism within the non-equilibrium Green function method. The Stoner gap was found to be created between the spin-majority channel and the spin-minority channel on LDOS of the hBN monoatomic boron-vacancy (V_B) near the vicinity of Fermi energy, creating a possible control of the spin valve by considering two different magnetic allignment of hBN(V_B) layers, anti-parallel and parallel configuration. The results of the transmission probability calculation showed a high electron transmission in the parallel configuration of the hBN(V_B) layers and a low transmission when the antiparallel configuration was considered. A high TMR ratio of approximately 400% was observed when comparing the antiparallel and parallel configuration of hBN(V_B) layers in the hBN (V_B)/Gr/hBN(V_B), giving the highest TMR for the thinnest MTJ system.

INTRODUCTION

Magnetic tunnel junctions (MTJs) have been extensively studied for their potential applications in spintronics, such as logic devices, hard drive magnetic read heads, and magnetic sensors [1–6]. The tunneling magnetoresistance (TMR) ratio is a key factor in improving MTJs, and MgO is the most common tunnel barrier used. CoFeB/MgO/CoFeB MTJs have achieved the highest TMR of 1100% at 4.2 K [7]. However, when the barrier thickness is reduced to downscale the device, the TMR can be reduced to 55% due to the presence of uncontrollable defects in the MgO tunnel barrier [8, 9].

Researchers have recently turned their attention to a 2D material-based magnetic junction for novel spintronics applications. 2D materials such as graphene or hBN have been used as a spin valve in the current-in-plane (CIP) scheme [10–13] by controlling its unique topological nature or have been used as non-magnetic spacers in current-perpendicular-to-plane (CPP) MTJs. While experimental data supporting the effectiveness of the former have not yet been confirmed, the latter has shown relatively low performance in the TMR ratio [14–24]. Previous studies show that the interface between the ferromagnetic electrode (FME) and 2D materials plays an

important role in transmission through the tunnel barrier [25–27]. When a conventional FME was created, that is, an electrode of a transition metal such as Fe, Ni, or Co, a chemisorption was created that resulted in a strong pd hybridization between 2D materials and FME [25–27]. This hybridization affects the transmission of electrons, especially when 2D polar materials, such as hBN, are used as a tunnel barrier. Strong pd hybridization at the interface leads to buckling of the hBN and creates a dipole moment at the interface. This dipole moment leads to the shift of Fermi energy from the peak of transmission through the d -orbital of FME, creating a small TMR ratio [25–27].

Several strategies have been proposed to avoid a strong pd -hybridization between FME and hBN, such as the introduction of transition metal FME alloys with inert metals such as Pt creating Co₃Pt alloy [25] or using MXene-based FME[28–30]. The occurrence of Pt in the alloy allows physisorption of hBN on the FME instead of chemisorption[25], creating a high transmission peak in parallel configuration (PC) at Fermi energy. Similarly, MXene-based FME, which usually consists of a rare-earth heavy-element metal such as Fe₃GeTe₂, creates a van der Waals interaction with hBN due to the relatively large atomic size and a more diffuse electron of heavy-elements

atom (Te atom) cloud compared to lighter elements[28]. However, creating and maintaining a long-range order of single-phase structure on the surface of Co_3Pt alloy or Fe_3GeTe_2 is rather challenging, especially at room temperature and high production cost [30–32].

On the other hand, the magnetic properties of hBN Boron-vacancy (V_B) has been a subject of significant research interest for the purpose of quantum computing applications [33–35]. Recent experiments recorded optically detected magnetic resonance (ODMR) signals at room temperature for color centers in hBN(V_B) [33]. In addition, distinct resonances are observed in the room-temperature ODMR spectrum even without an external magnetic field [34]. This observation further supports the presence of the magnetic moment associated with the V_B defect at room temperature. A first-principles study also supports the experimental results of the ODMR signals [35], confirming a possible magnetic moment on hBN(V_B) in room-temperature. Although relatively low photoluminescence and contrast of ODMR were found [36], which means that further research is necessary to enhance the ODMR sensitivity in hBN spin defects for the quantum computing application, the appearance of the magnetic moment on the hBN(V_B) becomes a possible key point to create a successful design of the thinnest MTJ using 2D materials.

In this work, we present a new strategy, employing light-element-based materials, to create a van der Waals-based MTJ with only a three-atom-layer thickness. Here, we proposed a three layer of hBN(V_B)/Graphene(Gr)/hBN(V_B) sandwiched structure. hBN (V_B) is used as the ferromagnetic layer that filters the transmission of electrons from two non-magnetic electrodes. The Gr layer is used between hBN (V_B) to keep transmission not too small due to the insulating nature of hBN [27]. The investigation of the magnetic properties and electronic structure of the system was performed using density functional theory (DFT), while the transmission probability of hBN(V_B)/Gr/hBN(V_B) MTJ was investigated using the Landauer–Büttiker (LB) formalism within the non-equilibrium Green function (NEGF) method. Our calculation results observed a high TMR ratio of about 400% in the hBN(V_B)/Gr/hBN(V_B) MTJ with Cu metal used as electrode. This results show the highest TMR ratio found in the thinnest MTJ system, which consists only of a three-atomic layer thickness.

COMPUTATIONAL METHOD

In this theoretical work, a supercell of 3×3 hBN layer with monoatomic atom B vacancy was considered, as shown in Figure 1(a). In the MTJ system, a Gr layer is sandwiched between hBN(V_B) layers, as shown in Figure 1(b). The most stable configuration of hBN/Gr/hBN

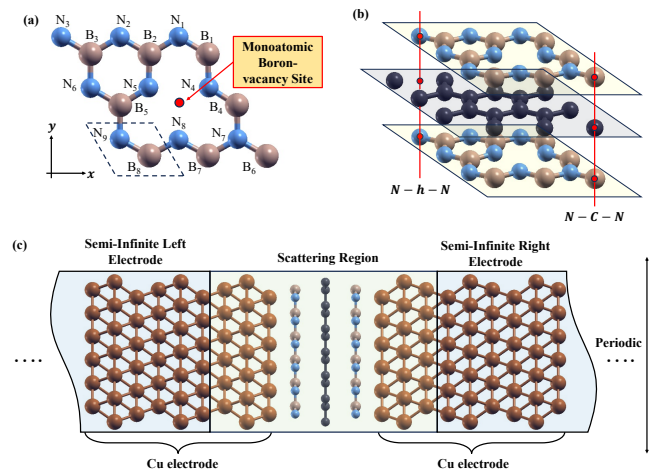


FIG. 1. (a) The crystal structure of hBN with Boron-vacancy. a 3×3 unit cell was used in the calculations which consists of nine atoms of Nitrogen and eight atoms of Boron. Blue (pink) color ball represents N (B) atoms. (b) hBN(V_B)/Gr/hBN(V_B) MTJ system where N atoms of hBN right on top and below hollow-site of Gr ($N-h-N$) and B atoms right on top and below of C atoms of Gr ($B-C-B$). The black color ball represent C atoms of graphene. (c) The setup to calculate the tunneling transmission probability of hBN(V_B)/Gr/hBN(V_B) MTJ where Cu is used as electrode. The scattering region consists of 3 layer Cu/hBN(V_B)/Gr/hBN(V_B)/3 layer Cu, while both left and right electrode consists of 6 layer of Cu.

was observed where the B atoms of the hBN were on top and below the C atoms of graphene, while the N atoms were right on top and below the hollow site of graphene[12, 27, 37]. Since the Boron monovacancy in hBN does not change much in the van der Waals interaction between hBN and graphene in 3×3 supercell, this stable stacking configuration was also applied on the hBN(V_B)/Gr/hBN(V_B) MTJ system, as shown in Figure 1(b). In the case of hBN(V_B)/Gr/hBN(V_B) MTJ investigation, both the antiparallel configuration (APC) and the parallel configuration (PC) were considered for the upper and lower hBN(V_B). In the case of APC, the magnetic moment orientation of the lower (upper) hBN(V_B) was fixed in the upward (downward) direction. On the other hand, both upper and lower hBN(V_B) magnetic moment orientations were fixed upward when the PC state was considered.

The SIESTA package [38, 39] was employed to calculate structural equilibrium, magnetic properties, spin-charge density mapping, and local density of states (LDOS) using spin-polarized DFT. The Troullier–Martins [40] pseudopotential and a revised Perdew–Burke–Ernzerhof functional for a densely packed solid surface (i.e., the PBESol functional) [41] were used to describe the electron–ion interaction within the generalized gradient approximation (GGA). A basis set with

double-zeta and polarization was utilized [42–44]. The atomic positions were relaxed with a 0.001 eV/Å force tolerance, and a $36 \times 36 \times 1$ Monkhorst–Pack k-mesh was employed for the calculations. An 800 Ry mesh cut-off was also used. Additionally, van der Waals interactions between hBN and graphene were taken into account by applying a Grimme-type dispersion potential [45].

The tunneling transmission probability will be calculated using the LB formalism within the NEGF method. First, the tunneling transmission probability will be done on hBN(V_B) to understand the capability of hBN(V_B) layer filtered the electron spin transmission through the CPP scheme. Subsequently, the tunneling transmission probability calculation was done on hBN(V_B)/Gr/hBN(V_B) MTJ. For the purpose of calculating the tunneling transmission probability, a Cu electrode is used in the calculation, which is a non-magnetic electrode, as shown in Figure 1(c). The spin-dependent current was calculated using the LB equation given by:

$$I^{\uparrow(\downarrow)} = \frac{e}{h} \int_{\min \infty}^{\infty} T^{\uparrow(\downarrow)}(E) [f_L(E, \mu) - f_R(E, \mu)] dE \quad (1)$$

where $f_L(E, \mu)$ ($f_R(E, \mu)$) is the right (left) moving electron injected from the left (right) lead in the form of the Fermi–Dirac function. μ_L (μ_R) denotes the chemical potentials of the left (right) electrodes. Since the zero bias voltage was considered, thus $\mu_L = \mu_R = E_F$. In addition, the ballistic transmission T as a function of energy E is described with respect to the Green function form as

$$T^{\uparrow(\downarrow)}(E) = \text{Tr} \left\{ \left[\Gamma_L G^R \Gamma_R G^A \right] \right\} \quad (2)$$

where Γ_L (Γ_R) is the coupling matrix of the left (right) electrode, G^R (G^A) is the retarded (advanced) Green functions of the central region.

Finally, in the hBN(V_B)/Gr/hBN(V_B) MTJ system, the MR ratio can be calculated by including the difference between the current in the APC and PC states and then dividing it by the current in the APC state as follows:

$$\text{TMR ratio} = \frac{I_{PC} - I_{APC}}{I_{APC}} \times 100\%. \quad (3)$$

RESULTS AND DISCUSSION

Magnetic, electronics, and transport properties of hBN(V_B) as spin-filter

The monoatomic Boron vacancy in the hBN layer was expected to give magnetization in the hBN due to the unpaired electron of the N atoms at the vacancy site due to

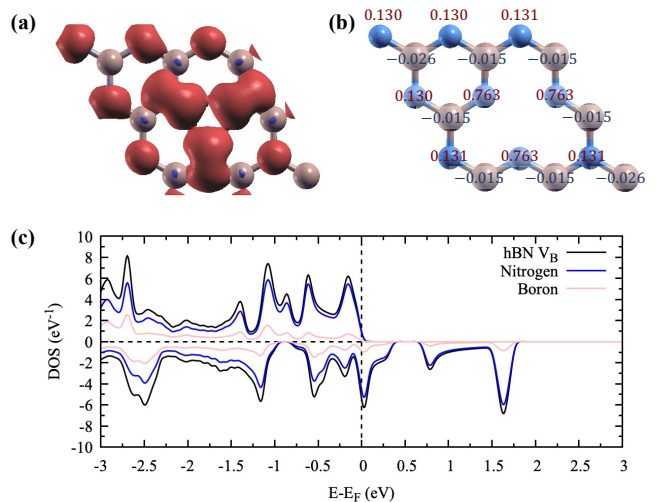


FIG. 2. (a) The hBN 3×3 V_B spin charge density mapping (SCDM) (red (blue) color represent spin-up (spin-down) electron density), (b) magnetic moment on each atoms (in μ_B unit; negative value corresponds to spin-down and positive value corresponds to spin-up), and (c) local density of states (LDOS). The positive (negative) value of DOS represents spin majority (minority) channel.

the absence of a σ -bond with the B atom. We performed spin charge density mapping (SCDM) to our proposed 3×3 hBN with monoatomic Boron vacancy to understand the distribution of spin-up and spin-down electron density. Figure 2(a) shows that the spin-up electron density dominates the hBN(V_B), due to our initial configuration of the system having a spin-up magnetization direction. From SCDM it shows that the spin-up electron density was found to be strong near the vacancy. However, the N atoms relatively far from the vacancy retain the strong spin-up electron density mapping, but the amplitude was reduced. Meanwhile, the B atoms have spin-down electron density, which is opposite to that of the N atoms. A small spin-down electron density was expected in the B atoms, since all valence electrons of the B atoms were used to create a σ -bond with the N atoms.

Figure 2(b) shows the magnetic moment of each atom in hBN(V_B). The magnetic moment of N atoms near the vacancy implies that the spin-up electron accumulated near the vacancy from the unpaired electron of N atoms has a magnetic moment around $1.5 \mu_B$. The remaining magnetic moment in N atoms at the vacancy, which around ≈ 0.263 comes from the unpaired electron at the p_z -orbital of N atoms. This result suggests that a ferromagnetic order was dominant between the magnetic moment near the vacancy and N atoms. The reduced value of the magnetic moment on N atoms, which are relatively far from vacancy, indicated a short range of magnetic exchange was created. Note that when a bigger supercell was considered, local ferromagnetism is expected in the hBN(V_B) layer, instead of creating a full

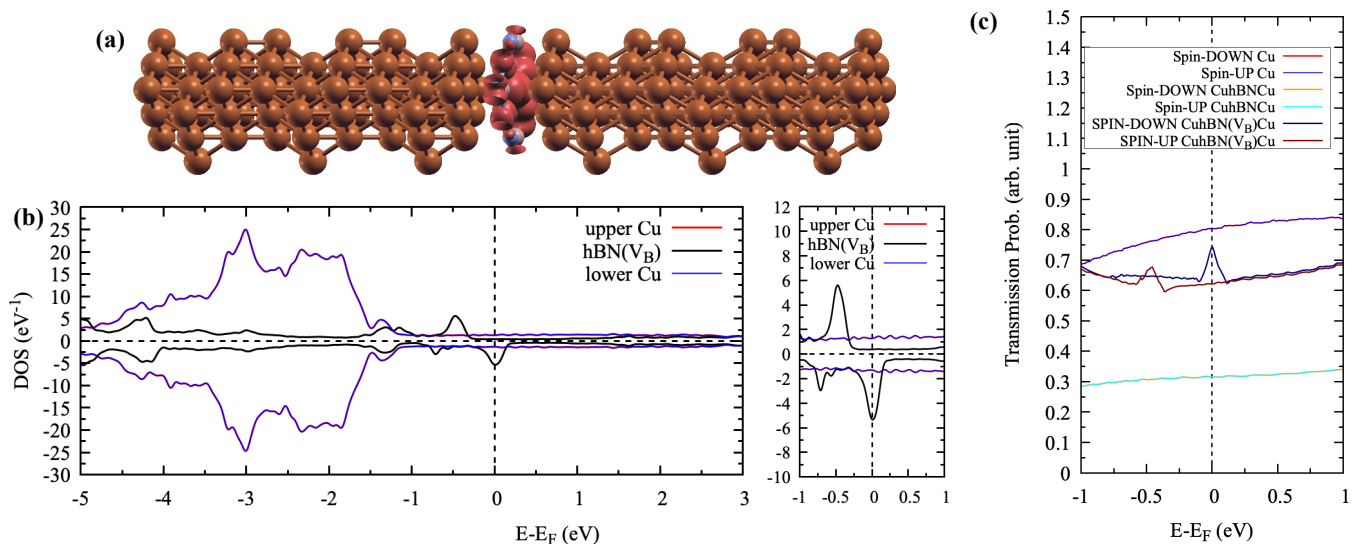


FIG. 3. (a) SCDM of 3×3 Cu/hBN(V_B)/Cu (red (blue) color represents spin-up (spin-down) electron density). (b) LDOS of 3×3 Cu/hBN(V_B)/Cu. The upper (lower)-Cu corresponds to the Cu layer right on top (below) of hBN(V_B). The positive (negative) value of DOS represents the spin majority (minority) channel. (c) Tunneling transmission probability of Cu/hBN(V_B)/Cu with Cu/hBN/Cu and pristine Cu transmission probability as a reference.

ferromagnetic layer.

The LDOS of the 3×3 hBN(V_B) layer was shown in Figure 2(c). The DOS of state near Fermi energy shows that the Stoner gap was created between the spin majority channel and the spin minority channel. Since the magnetic moment direction was set to spin-up direction, the spin majority channel has shifted to a lower energy, creating a higher occupied state compared to the spin minority channel. In the spin-majority channel, the huge band gap was observed from the Fermi energy to the higher energy, which represents a typical huge band gap of hBN and represents its insulating nature. However, in the spin minority channel, additional states were shown to be created from 0.6 eV to 1.8 eV. This localized state in the middle of the hBN insulator gap corresponds to the localized state of the vacancy. Since the magnetic moment was set into a spin-up direction, the localized state at the insulator gap of hBN in the spin minority channel is unoccupied (at an energy higher than the Fermi energy). Furthermore, it is also shown that this localized state was mainly coming from the N atoms by looking at the LDOS of the N atoms in the hBN (V_B) layer.

The Stoner gap found in the DOS of hBN becomes a potential aspect to be used for electron spin filter when a non-magnetic electrode is connected, creating a CPP scheme of electron transport. At the Fermi energy, it was shown that a high-spin filter is possible where the spin-majority channel has lower density while, oppositely, the spin-minority channel has high density. To explore this possibility, a tunneling transmission probability was carried out on the 3×3 hBN(V_B) by connecting it to the Cu electrode on the upper and lower part, as shown in Fig-

ure 3(a). When the hBN layer comes into contact with the Cu layer, a physisorption between the Cu/hBN interface is expected [25]. This physisorption at the Cu/hBN interface was also applied at the Cu/hBN(V_B) where the interlayer distance between Cu at the interface and hBN is around 2.51Å.

When Cu/hBN has a physisorption interface, although no hybridization was created between Cu and hBN, a proximity effect was observed on the hBN layer, changing the electronic structure from an insulator to a metal (see Section III Supplementary Materials). This proximity effect was also found in physisorption at the interface of Cu/hBN(V_B). The LDOS of hBN in Cu/hBN(V_B)/Cu shows a small but non-zero density of states near the Fermi energy, as shown in Figure 3(b), indicating a metal electronic structure. However, although the proximity effect changes the hBN(V_B) slightly metallic, the induced magnetic moment on hBN(V_B) still kept as shown in Figure 3(a) where there is a clear spin-up charge density on hBN(V_B). This is also confirmed by the Stoner gap created on the hBN(V_B) LDOS, especially near the Fermi energy, as shown on the right side of Figure 3(b). It is also shown that the DOS from the vacancy site still survives, creating two DOS peak on the hBN (V_B) LDOS at Fermi energy ($E - E_F = -0.5$ eV) for the spin minority (majority) channel. It should be noted in Figure 3(a) that the induced magnetization on hBN due to the vacancy does not give rise to an induced magnetic moment on the Cu layer even at the interface. Figure 3(b) also shows that no Stoner gap was created in the Cu layers (both at the top and below hBN(V_B)), implying no magnetic moment was induced on the Cu layer at the

interface.

The Stoner gap in the $\text{hBN}(V_B)$ LDOS at the interface is expected to give a spin-filter effect when current flows from the left electrode to the right electrode (vice versa). The calculation of the tunneling transmission probability on $\text{Cu}/\text{hBN}(V_B)/\text{Cu}$ shown in Figure 3(c) suggests a spin filter effect at the Fermi energy. This spin-filter was mediated by the localized state of the vacancy site, since the peak transmission of the spin-down (spin-up) electron corresponds to the LDOS of the vacancy site in the spin minority (majority) channel. Furthermore, by comparing the transmission probability of pristine Cu, $\text{Cu}/\text{hBN}/\text{Cu}$, and $\text{Cu}/\text{hBN}(V_B)/\text{Cu}$, the localized state of the vacancy site transmit electron is more efficient than that of pristine hBN, shown by the slight reduction in the transmission probability of the electron compared to that of pristine Cu. The efficient spin-filter mediated by the localized state of $\text{hBN}(V_B)$ gives a prospective spin-valve device when a sandwiched structure of $\text{hBN}(V_B)/\text{Gr}/\text{hBN}(V_B)$ is considered, which is discussed in the next section.

The high tunneling magnetoresistance ratio on $\text{hBN}(V_B)/\text{Gr}/\text{hBN}(V_B)$ MTJ

To create an MTJ system based on $\text{hBN}(V_B)$, $\text{hBN}(V_B)/\text{Gr}/\text{hBN}(V_B)$ was considered. Two magnetic configurations of antiparallel configuration (APC) and parallel configuration (PC) of the upper and lower $\text{hBN}(V_B)$ layers were considered. The SCDM of both magnetic configurations is shown in Figures 4 (a) and (b). The lowest energetically magnetic configuration is the PC state, with the total energy difference between the APC and the PC state with respect to the APC state (ΔE_{APC-PC}) being 23.565 meV. Furthermore, the SCDM of both APC and PC states shows that no magnetic moment is induced on the Gr layer. This implies that the localized state of the vacancy in $\text{hBN}(V_B)$ does not give a magnetic proximity effect on graphene.

The LDOS of $\text{hBN}(V_B)/\text{Gr}/\text{hBN}(V_B)$ in figure 4(c) and (d) for the APC and PC states, respectively, shows that no proximity effect is also found in the LDOS of the Gr layer. This was shown from the localized state of $\text{hBN}(V_B)$ from $E - E_F = 0.5$ eV to 1.8 eV in the spin minority channel, which does not affect the graphene LDOS in the same energy range. However, from the LDOS of Gr, the Gr layer gave a small magnetic response due to the magnetic configuration of the $\text{hBN}(V_B)$ layers. In the case of APC, the Gr LDOS of the spin majority and minority channels is the same, indicating no magnetic response on the Gr layer. However, in the PC state, a small Stoner gap was observed, indicating the magnetic response of the Gr layer due to the magnetization of $\text{hBN}(V_B)$ from both the upper and lower sides. Furthermore, the small mass-gapped Dirac cone of graphene

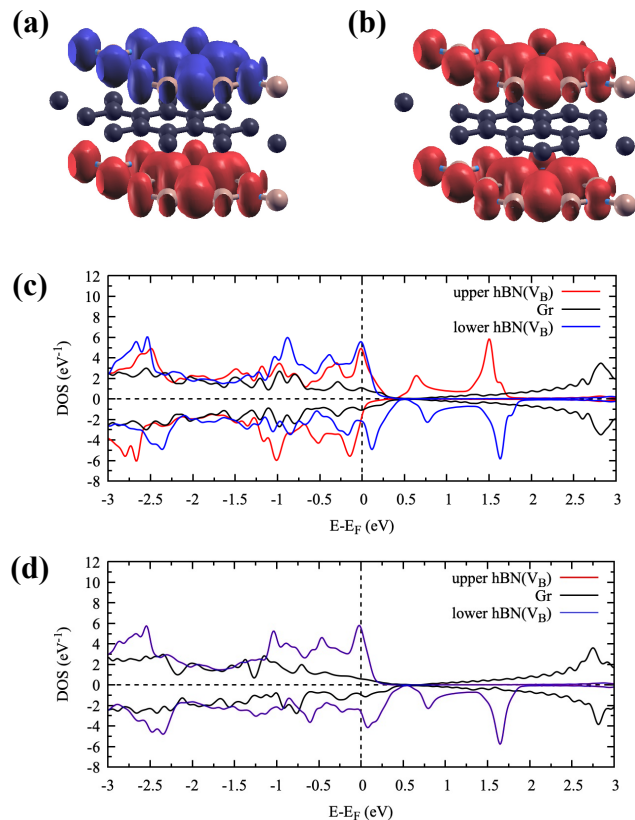


FIG. 4. The SCDM of 3×3 $\text{hBN}(V_B)/\text{Gr}/\text{hBN}(V_B)$ for (a) APC and (b) PC states (red (blue) color represent spin-up (spin-down) electron density). LDOS of 3×3 $\text{hBN}(V_B)/\text{Gr}/\text{hBN}(V_B)$ for (c) APC and (d) PC states. The positive (negative) value of DOS represents spin majority (minority) channel.

appeared in both APC and PC states, which is consistent with a previous study [37]. This is due to the fact that the B atoms of $\text{hBN}(V_B)$ were located on top and below one of the C atoms of graphene, slightly modulating the potential between the C atoms sublattice A and B of graphene. However, here a small shift of the mass-gapped Dirac cone of graphene was observed from zero energy to 0.5 eV, which could come from the doping effect $\text{hBN}(V_B)$.

The perfect spin-valve LDOS from $E - E_F = 0.5$ eV to 1.8 eV in $\text{hBN}(V_B)/\text{Gr}/\text{hBN}(V_B)$ are expected to give a high efficiency of the TMR ratio. By connecting the $\text{hBN}(V_B)/\text{Gr}/\text{hBN}(V_B)$ MTJ with the Cu electrode, the CPP transmission probability of $\text{Cu}/\text{hBN}(V_B)/\text{Gr}/\text{hBN}(V_B)/\text{Cu}$ was investigated. Investigation was done first at $\text{Cu}/\text{hBN}(V_B)/\text{Gr}/\text{hBN}(V_B)/\text{Cu}$ in APC state. The SCDM of the system shown in Figure 5(a) suggests that there is no induced magnetic moment on the Cu layer at the interface, the same as in the case of $\text{Cu}/\text{hBN}(V_B)/\text{Cu}$. The LDOS of $\text{hBN}(V_B)$ and Gr layers in $\text{Cu}/\text{hBN}(V_B)/\text{Gr}/\text{hBN}(V_B)/\text{Cu}$ was

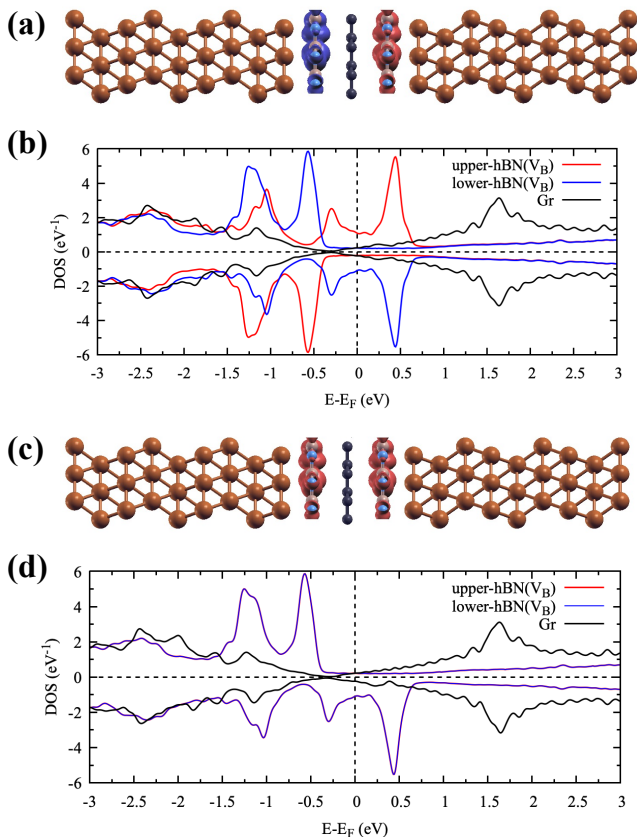


FIG. 5. SCDM of 3×3 Cu/hBN(V_B)/Gr/hBN(V_B)/Cu for (a) APC and (c) PC states (red (blue) color represents spin-up (spin-down) electron density). LDOS of 3×3 Cu/hBN(V_B)/Gr/hBN(V_B)/Cu for (b) APC and (d) PC states. The positive (negative) value of DOS represents the spin majority (minority) channel.

shown in Figure 5(b). Unlike the LDOS of Gr in hBN(V_B)/Gr/hBN(V_B) where small mass-gapped Dirac cone was observed, in Cu/hBN(V_B)/Gr/hBN(V_B)/Cu Gr layer keep its Dirac cone. This is due to the difference in the distance between layers between hBN(V_B) and the Gr layer in hBN(V_B)/Gr/hBN(V_B) and Cu/hBN(V_B)/Gr/hBN(V_B)/Cu which 2.83 Å and 2.88 Å, respectively. Furthermore, it was shown that the Fermi energy in Cu/hBN(V_B)/Gr/hBN(V_B)/Cu is shifted to the higher energy compare to hBN(V_B)/Gr/hBN(V_B). This shift could come from the surface state of the Cu electrode, giving the electron-doped effect to hBN(V_B)/Gr/hBN(V_B) (See Supplementary Materials). Although there is small additional LDOS due to the proximity effect of Cu on hBN(V_B), the opposite high intensity between the majority of spin and the minority channel near the vicinity of Fermi energy is still prominent and is expected to give electrons a low transmission probability. This low transmission probability was confirmed in Figure 6(a).

When considering the PC state, similarly, the SCDM

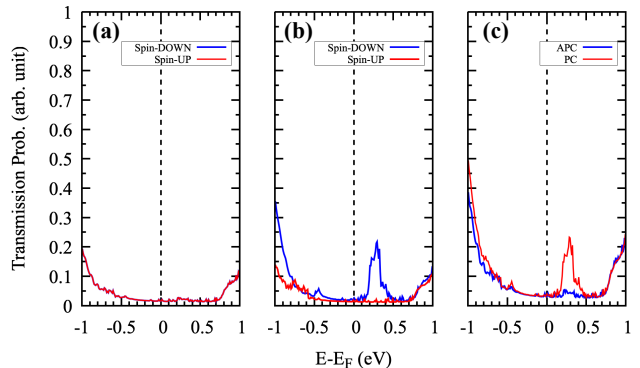


FIG. 6. Tunneling transmission probability of Cu/hBN(V_B)/Gr/hBN(V_B)/Cu for (a) APC and (b) PC states, and (c) the comparison between both of them.

of the system shown in Figure 5(c) suggests that there is no induced magnetic moment in the Cu layer at the interface. From the LDOS, it also shows the absence of a graphene mass-gapped Dirac cone due to the increase of the interlayer distance between hBN(V_B) and the Gr layer and the shift of Fermi energy due to the electron-doped effect of the surface state of the Cu electrode. However, in this PC state, the upper and lower hBN(V_B) spin majority and minority channels have the same LDOS, creating a high possible transmission of electrons, especially at the DOS peak near 0.4 eV. This high transmission probability around 0.4 eV was confirmed in Figure 6(b). Finally, when comparing the total transmission probability of APC with the PC state, a high TMR ratio $\approx 400\%$ was shown in Figure 6(c). This high transmission probability was achieved by only considering the three-atomic thickness of MTJ based on 2D materials.

The interchange between the PC and the APC states can be considered utilizing the small energy difference of 23.565 meV. The PC state was previously found to be the most stable magnetic alignment between the upper and lower hBN(V_B) layers. Thus, to consider the APC state, the magnetic moment of one of the hBN(V_B) layers needs to flip to have an opposite direction. One of the methods that can be used is the spin accumulation effect on the Cu surface through spin vorticity coupling of the oxidized Cu [46, 47]. When an in-plane current is given to oxidized Cu in a certain direction, spin accumulates on the surface of Cu near hBN(V_B), giving a magnetic field in the opposite direction of another hBN(V_B) layer. To change the magnetic moment configuration back to PC, an opposite in-plane current is introduced on oxidized Cu, creating the same spin direction accumulated on the surface of Cu near hBN(V_B). In addition, the small energy difference between the APC and PC states indicates that a small current was needed to change the magnetic configuration, resulting in a low-energy-consumption MTJ device.

This $\text{hBN}(V_B)/\text{Gr}/\text{hBN}(V_B)$ can be fabricated using various methods; one of which involves employing chemical vapor deposition (CVD) to create a stack layer of $\text{hBN} / \text{Gr} / \text{hBN}$ [48–50] and introducing a monoatomic vacancy on hBN using Ar ion sputtering [51]. Initially, hBN CVD growth on the clean surface of $\text{Cu}(111)$ substrate can be achieved by introducing common Boron and Nitrogen precursors such as Boron trichloride (BCl_3) or Boron trifluoride (BF_3) and Ammonia (NH_3), respectively. Subsequently, a monoatomic vacancy was introduced on the pristine hBN layer by using Ar-ion sputtering. Following this, the Gr layer was grown on hBN by introducing precursor gases of carbon atoms, such as methane (CH_4) or ethylene (C_2H_4). And finally, the second $\text{hBN}(V_B)$ is grown in the same manner as the first $\text{hBN}(V_B)$.

CONCLUSION

In this work, we proposed a novel three-atom-layer van der Waals-based MTJ utilizing boron-vacancy defects in hBN . The approach involves employing both DFT for calculating electronic and magnetic properties and the LB formalism within the NEGF method to determine the MTJ's transmission probability. Our findings observed the formation of a Stoner gap between the spin-majority and spin-minority channels on the LDOS of $\text{hBN}(V_B)$ near the Fermi energy. This enables control over the spin-valve behavior by manipulating the magnetic alignment (APC and PC) of the $\text{hBN}(V_B)$ layers. The results showed that the PC state exhibits high electron transmission, whereas the APC state results in low electron transmission, resulting in a remarkable TMR ratio of approximately 400%. These findings suggest promising prospects for developing high-performance spintronics devices with the proposed three-atom-layer MTJ design.

ACKNOWLEDGEMENTS

Calculations were performed at the Kyushu University computer center. H.H. gratefully acknowledges the fellowship support from the JSPS. This study was partly supported by the Japan Society for the Promotion of Science (JSPS) KAKENHI (Grant Nos. JP19H00862 and JP16H00914 in the Science of Atomic Layers, 21J22520 in the Grant-in-Aid for Young Scientists, and JP18K03456).

* Corresponding author: harfah.h@opt.mp.es.osaka-u.ac.jp; These authors contributed equally to this work

† These authors contributed equally to this work

- [1] C. Chappert, A. Fert, and F. N. Van Dau, The emergence of spin electronics in data storage, *Nature Materials* **6**, 813 EP (2007).
- [2] H. Dery, P. Dalal, L. Cywiński, and L. J. Sham, Spin-based logic in semiconductors for reconfigurable large-scale circuits, *Nature* **447**, 573 EP (2007).
- [3] J.-G. J. Zhu and C. Park, Magnetic tunnel junctions, *Materials Today* **9**, 36 (2006).
- [4] J. R. Childress and R. E. Fontana, Magnetic recording read head sensor technology, *Spintronics*, *Comptes Rendus Physique* **6**, 997 (2005).
- [5] E. Chen, D. Apalkov, Z. Diao, A. Driskill-Smith, D. Druist, D. Lottis, V. Nikitin, X. Tang, S. Watts, S. Wang, S. A. Wolf, A. W. Ghosh, J. W. Lu, S. J. Poon, M. Stan, W. H. Butler, S. Gupta, C. K. A. Mewes, T. Mewes, and P. B. Visscher, Advances and future prospects of spin-transfer torque random access memory, *IEEE Transactions on Magnetics*, *IEEE Transactions on Magnetics* **46**, 1873 (2010).
- [6] M. Iqbal, N. Qureshi, and G. Khan, *Recent Advancements in 2D-Materials Interface Based Magnetic Junctions for Spintronics*, Vol. 457 (Elsevier, 2018).
- [7] S. Ikeda, K. Miura, H. Yamamoto, K. Mizunuma, H. D. Gan, M. Endo, S. Kanai, J. Hayakawa, F. Matsukura, and H. Ohno, A perpendicular-anisotropy coFeB/MgO magnetic tunnel junction, *Nature Materials* **9**, 721 (2010).
- [8] J. C. Leutenantsmeyer, M. Walter, V. Zbarsky, M. Müntzenberg, R. R. Gareev, K. Rott, A. Thomas, G. Reiss, P. Peretzki, H. Schuhmann, M. Seibt, M. Czerner, and C. Heiliger, Parameter space for thermal spin-transfer torque, *Spin* **03**, 1350002 (2013).
- [9] W. X. Wang, Y. Yang, H. Naganuma, Y. Ando, R. Yu, and X. F. Han, The perpendicular anisotropy of $\text{Co}_40\text{Fe}_40\text{B}_{20}$ sandwiched between Ta and MgO layers and its application in $\text{CoFeB}/\text{MgO}/\text{CoFeB}$ tunnel junction, *Applied Physics Letters* **99**, 10.1063/1.3605564 (2011).
- [10] Y. Wicaksono, S. Teranishi, K. Nishiguchi, and K. Kusakabe, Tunable induced magnetic moment and in-plane conductance of graphene in $\text{Ni}/\text{graphene}/\text{Ni}$ nano-spin-valve-like structure: a first principles study, *Carbon* **143**, 828 (2019).
- [11] Y. Wicaksono, H. Harfah, G. K. Sunnardianto, M. A. Majidi, and K. Kusakabe, Colossal in-plane magnetoresistance ratio of graphene sandwiched with Ni nanostructures, *RSC Advances* **12**, 13985 (2022).
- [12] Y. Wicaksono, H. Harfah, G. K. Sunnardianto, M. A. Majidi, and K. Kusakabe, Spin-topological electronic valve in $\text{Ni}/\text{hBN}-\text{graphene}-\text{hBN}/\text{Ni}$ magnetic junction, *Magnetochemistry* **9**, 113 (2023).
- [13] N. Morishita, G. K. Sunnardianto, S. Miyao, and K. Kusakabe, Theoretical analysis of pseudodegenerate zero-energy modes in vacancy-centered hexagonal armchair nanographene, *Journal of the Physical Society of Japan* **85**, 084703 (2016).
- [14] M. Piquemal-Banci, R. Galceran, M.-B. Martin, F. Godel, A. Anane, F. Petroff, B. Dlubak, and P. Senor, 2d-MTJs: introducing 2d materials in magnetic tunnel junctions, *Journal of Physics D: Applied Physics* **50**, 203002 (2017).
- [15] T. M. G. Mohiuddin, E. Hill, D. Elias, A. Zhukov, K. Novoselov, and A. Geim, Graphene in multilayered c_{60} spin valves, *IEEE Transactions on Magnetics* **44**, 2624 (2008).

- [16] P. U. Asshoff, J. L. Sambricio, A. P. Rooney, S. Slizovskiy, A. Mishchenko, A. M. Rakowski, E. W. Hill, A. K. Geim, S. J. Haigh, V. I. Fal'ko, I. J. Vera-Marun, and I. V. Grigorieva, Magnetoresistance of vertical co-graphene-niFe junctions controlled by charge transfer and proximity-induced spin splitting in graphene, *2D Materials* **4**, 031004 (2017).
- [17] M. Z. Iqbal, M. W. Iqbal, X. Jin, C. Hwang, and J. Eom, Interlayer dependent polarity of magnetoresistance in graphene spin valves, *J. Mater. Chem. C* **3**, 298 (2015).
- [18] M. Z. Iqbal, M. W. Iqbal, J. H. Lee, Y. S. Kim, S.-H. Chun, and J. Eom, Spin valve effect of nife/graphene/nife junctions, *Nano Research* **6**, 373 (2013).
- [19] J.-J. Chen, J. Meng, Y.-B. Zhou, H.-C. Wu, Y.-Q. Bie, Z.-M. Liao, and D.-P. Yu, Layer-by-layer assembly of vertically conducting graphene devices, *Nature Communications* **4**, 1921 (2013), article.
- [20] F. Li, T. Li, and X. Guo, Vertical graphene spin valves based on $\text{La}_2/\text{3Sr}_1/\text{3MnO}_3$ electrodes, *ACS Applied Materials & Interfaces* **6**, 1187 (2014).
- [21] W. Li, L. Xue, H. D. Abruña, and D. C. Ralph, Magnetic tunnel junctions with single-layer-graphene tunnel barriers, *Phys. Rev. B* **89**, 184418 (2014).
- [22] S. Mandal and S. K. Saha, Ni/graphene/nif nanostructures for spintronic applications, *Nanoscale* **4**, 986 (2012).
- [23] M.-B. Martin, B. Dlubak, R. S. Weatherup, M. Piquemal-Banci, H. Yang, R. Blume, R. Schloegl, S. Collin, F. Petroff, S. Hofmann, J. Robertson, A. Anane, A. Fert, and P. Seneor, Protecting nickel with graphene spin-filtering membranes: A single layer is enough, *Applied Physics Letters* **107**, 012408 (2015), <https://doi.org/10.1063/1.4923401>.
- [24] S. Entani, T. Seki, Y. Sakuraba, T. Yamamoto, S. Takahashi, H. Naramoto, K. Takanashi, and S. Sakai, Magnetoresistance effect in $\text{Fe}_2\text{O}_3/\text{graphene}/\text{Fe}_2\text{O}_3$ vertical spin valves, *Applied Physics Letters*, *Applied Physics Letters* **109**, 082406 (2016).
- [25] H. Lu, Y. Guo, and J. Robertson, ab initio study of hexagonal boron nitride as the tunnel barrier in magnetic tunnel junctions, *ACS Applied Materials Interfaces* **13**, 47226 (2021).
- [26] H. Harfah, Y. Wicaksono, M. A. Majidi, and K. Kusakabe, Spin-current control by induced electric polarization reversal in ni/hbn/ni: A cross-correlation material, *ACS Applied Electronic Materials*, *ACS Applied Electronic Materials* **2**, 1689 (2020).
- [27] H. Harfah, Y. Wicaksono, G. K. Sunnardianto, M. A. Majidi, and K. Kusakabe, High magnetoresistance of a hexagonal boron nitride-graphene heterostructure-based mtj through excited-electron transmission, *Nanoscale Advances* **4**, 117 (2022).
- [28] Z. Wang, D. Sapkota, T. Taniguchi, K. Watanabe, D. Mandrus, and A. F. Morpurgo, Tunneling spin valves based on $\text{Fe}_3\text{GeTe}_2/\text{hbn}/\text{Fe}_3\text{GeTe}_2$ van der Waals heterostructures, *Nano Letters* **18**, 4303 (2018).
- [29] J. Wen, G. Zhang, H. Wu, L. Yang, W. F. Zhang, and H. Chang, Room-temperature and tunable tunneling magnetoresistance in Fe_3GeTe_2 -based 2d van der Waals heterojunctions, *ACS Applied Materials Interfaces* **15**, 36519 (2023).
- [30] H. Zhou, Y. Zhang, and W. Zhao, Tunable tunneling magnetoresistance in van der Waals magnetic tunnel junctions with 1T-CrTe_2 electrodes, *ACS Applied Materials Interfaces* **13**, 1214 (2020).
- [31] A. Front and C. Mottet, Ordering frustration in large-scale co-opt nanoalloys, *The Journal of Physical Chemistry C* **125**, 16358 (2021).
- [32] L. Liu, C. Zhou, T. Zhao, B. Yao, J. Zhou, X. Shu, S. Shi, S. Xi, D. Lan, W. Lin, Q. Xie, L. Ren, Z. Liu, C. Sun, P. Yang, E. Guo, Z. L. Dong, A. Manchon, and J. Chen, Current-induced self-switching of perpendicular magnetization in copt single layer, *Nature Communications* **13**, 10.1038/s41467-022-31167-w (2022).
- [33] T. T. Tran, C. Elbadawi, D. Totonjian, C. Lobo, G. Grosso, H. Moon, D. Englund, M. J. Ford, I. Aharonovich, and M. Toth, Robust multicolor single photon emission from point defects in hexagonal boron nitride, *ACS Nano* **10**, 7331 (2016).
- [34] W. Liu, Z. Li, Y. Yang, S. Yu, Y. Meng, Z. Wang, Z. Li, N. Guo, F. Yan, Q. Li, J. Wang, J. Xu, Y. Wang, J. Tang, C. Li, and G. Guo, Temperature-dependent energy-level shifts of spin defects in hexagonal boron nitride, *ACS Photonics* **8**, 1889 (2021).
- [35] V. Ivády, G. Barcza, G. Thiering, S. Li, H. Hamdi, J.-P. Chou, Ö. Legeza, and A. Gali, Ab initio theory of the negatively charged boron vacancy qubit in hexagonal boron nitride, *npj Computational Materials* **6**, 41 (2020).
- [36] Z. Mu, H. Cai, D. Chen, J. Kenny, Z. Jiang, S. Ru, X. Lyu, T. S. Koh, X. Liu, I. Aharonovich, and W. Gao, Excited-state optically detected magnetic resonance of spin defects in hexagonal boron nitride, *Phys. Rev. Lett.* **128**, 216402 (2022).
- [37] R. Quhe, J. Zheng, G. Luo, Q. Liu, R. Qin, J. Zhou, D. Yu, S. Nagase, W.-N. Mei, Z. Gao, and J. Lu, Tunable and sizable band gap of single-layer graphene sandwiched between hexagonal boron nitride, *NPG Asia Materials* **4**, e6 (2012).
- [38] D. Sánchez-Portal, P. Ordejón, E. Artacho, and J. M. Soler, Density-functional method for very large systems with lcao basis sets, *International Journal of Quantum Chemistry*, *International Journal of Quantum Chemistry* **65**, 453 (1997).
- [39] J. M. Soler, E. Artacho, J. D. Gale, A. García, J. Junquera, P. Ordejón, and D. Sánchez-Portal, The siesta method for ab initio order-n materials simulation, *Journal of Physics: Condensed Matter* **14**, 2745 (2002).
- [40] N. Troullier and J. Martins, Efficient pseudopotentials for plane-wave calculations, *Physical Review B* **43**, 1993 (1991).
- [41] J. P. Perdew, A. Ruzsinszky, G. I. Csonka, O. A. Vydrov, G. E. Scuseria, L. A. Constantin, X. Zhou, and K. Burke, Restoring the density-gradient expansion for exchange in solids and surfaces, *Phys. Rev. Lett.* **100**, 136406 (2008).
- [42] T. Ozaki and H. Kino, Numerical atomic basis orbitals from h to kr, *Physical Review B* **69**, 195113 (2004).
- [43] T. Ozaki, Variationally optimized atomic orbitals for large-scale electronic structures, *Physical Review B* **67**, 155108 (2003).
- [44] D. Sánchez-Portal, E. Artacho, and J. Soler, Analysis of atomic orbital basis sets from the projection of plane-wave results, *Journal of Physics: Condensed Matter* **8**, 3859 (1996).
- [45] S. Grimme, Semiempirical gga-type density functional constructed with a long-range dispersion correction, *Journal of Computational Chemistry* **27**, 1787 (2006).
- [46] G. Tatara, Hydrodynamic theory of vorticity-induced spin transport, *Phys. Rev. B* **104**, 184414 (2021).

- [47] G. Okano, M. Matsuo, Y. Ohnuma, S. Maekawa, and Y. Nozaki, Nonreciprocal spin current generation in surface-oxidized copper films, *Phys. Rev. Lett.* **122**, 217701 (2019).
- [48] A. V. Kretinin, Y. Cao, J. S. Tu, G. L. Yu, R. Jalil, K. S. Novoselov, S. J. Haigh, A. Gholinia, A. Mishchenko, M. Lozada, T. Georgiou, C. R. Woods, F. Withers, P. Blake, G. Eda, A. Wirsig, C. Hucho, K. Watanabe, T. Taniguchi, A. K. Geim, and R. V. Gorbachev, Electronic properties of graphene encapsulated with different two-dimensional atomic crystals, *Nano Letters* **14**, 3270 (2014).
- [49] J. S. Lee, S. H. Choi, S. J. Yun, Y. I. Kim, S. Boandoh, J.-H. Park, B. G. Shin, H. Ko, S. H. Lee, Y.-M. Kim, Y. H. Lee, K. K. Kim, and S. M. Kim, Wafer-scale single-crystal hexagonal boron nitride film via self-collimated grain formation, *Science* **362**, 817 (2018).
- [50] K. K. Kim, H. S. Lee, and Y. H. Lee, Synthesis of hexagonal boron nitride heterostructures for 2d van der waals electronics, *Chemical Society Reviews* **47**, 6342 (2018).
- [51] M. Ziatdinov, S. Fujii, K. Kusakabe, M. Kiguchi, T. Mori, and T. Enoki, Direct imaging of monovacancy-hydrogen complexes in a single graphitic layer, *Phys. Rev. B* **89**, 155405 (2014).